JOURNAL OF AIRCRAFT
Vol. 44, No. 5, September–October 2007

Computational Study of Submerged Air Inlet Performance Improvement Using Vortex Generators

César Celis Pérez,* Sandro Barros Ferreira,† and Luís Fernando Figueira da Silva‡
Pontifícia Universidade Católica do Rio de Janeiro,
22453-900 Rio de Janeiro, Rio de Janeiro, Brazil
and
Antonio Batista de Jesus§ and Guilherme Lara Oliveira¶
Empresa Brasileira de Aeronáutica, 12227-901 São José dos Campos, São Paolo, Brazil

DOI: 10.2514/1.25036

In this computational work, the influence of a delta wing vortex generator on the boundary layer that develops upstream of a submerged air intake is studied. The state-of-the-art analysis and design of these intakes is discussed in detail. The flow in a conventional NACA inlet is analyzed numerically and its results are considered as a reference for the cases in which the vortex generator is included. A delta wing vortex generator is designed and mounted to the conventional NACA inlet, and the result of this configuration is studied through parametric variations of the vortex generator geometry. Finally, a support mast of the vortex generator is designed and included in the model, and simulations are performed for the configuration NACA inlet with vortex generator and mast. Three sideslip angles are considered for the mast. The results show that the use of the delta wing vortex generator is responsible for considerable reductions of the boundary-layer thickness and, consequently, significant improvements of the performance parameters of the NACA inlet. The improvements relative to the conventional NACA intake in terms of ram-recovery ratio and mass flow rate are of up to 53 and 19%, respectively.

Nomenclature

A	=	area
C	=	chord
C_D	=	drag coefficient
C_{Dfl}	=	submerged inlet drag coefficient
C_L	=	lift coefficient
D	=	total drag
HD	=	horizontal distance between the trailing edge of the vortex generator and the beginning of the ramp
$\dot{m}$	=	mass flow rate
p	=	static pressure
p_t	=	total pressure
Re	=	Reynolds number
S	=	span
V	=	flow velocity
α	=	angle of attack
β	=	sideslip angle
η_{fl}	=	ram-recovery ratio
Λ	=	aspect ratio
ρ	=	density
υ	=	dynamic viscosity

Subscripts

TH	=	throat plane
0	=	freestream conditions

Received 13 September 2006; revision received 24 November 2006; accepted for publication 28 November 2006.

*Graduate Student, Department of Mechanical Engineering, Rua Marquês de São Vicente, 225.
†Project Manager, Institute of Energy, Rua Marquês de São Vicente, 225.
‡Visiting Professor, Department of Mechanical Engineering, Rua Marquês de São Vicente, 225. Senior Member AIAA.
§Propulsion Systems Engineer, Avenida Brigadeiro Faria Lima, 2170.
¶Propulsion Systems Engineer, Avenida Brigadeiro Faria Lima, 2170.

I. Introduction

NACA intakes (Fig. 1) have been widely used in aircraft as a low drag source of external flow for air conditioning, ventilation, and cooling systems. The design criteria of these intakes were established during the 1940s and 1950s. Recently, classical aircraft intakes have been revisited with the use of computational fluid dynamic techniques (CFD), aiming to improve their performance, mainly with the use of the following techniques: 1) vortex generators [1,2], 2) flow deflectors [3,4], 3) parametric geometric optimization [5], and 4) pulsating jets [6]. None of the performance-enhancement techniques explored to date has shown decisive advantages with respect to the others.

The boundary-layer thickness upstream of the air intake is the key parameter governing the performance of this type of inlet [2,3,7]; the larger the boundary-layer thickness, the poorer the performance of the air inlet.

Delta wings are usually employed in supersonic airplanes, because they induce low wave drag while yielding high values of lift coefficient. These high values of lift coefficient are associated with the high levels of vorticity produced by the leading edge vortex generated along the suction side of the delta wing. In this work, the vortex generated by the delta wing will be shown to reduce the boundary-layer thickness through the mixing of high-momentum air from the freestream flow with the low-energy boundary-layer air.

The goal of this work is to evaluate the influence of delta wing vortex generators on the development of the boundary layer upstream of the inlet and, more specifically, on the performance parameters of the NACA intake. These performance parameters are the ram-recovery ratio, mass flow rate, and drag coefficient. Three parametric variations of the vortex generator (VG) geometry are studied: horizontal positioning, angle of attack, and area of the vortex generator. A support mast of the vortex generator is designed, and simulations are also performed of the ensemble NACA inlet with vortex generator and mast for three sideslip angles of the support. Before the discussion of the results, a review of state-of-the-art submerged inlets is presented, followed by a description of the computational modeling approach.

Fig. 1 Conventional NACA inlet [1].

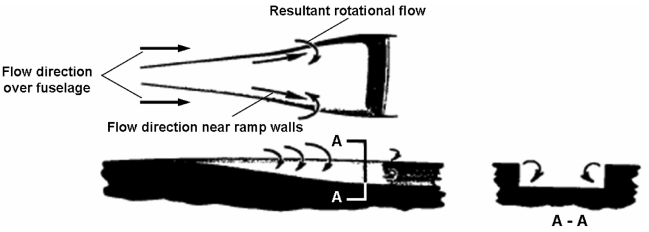

Fig. 3 Schematic representation of the rotational flow along a typical NACA inlet [4].

II. State of the Art

A. Initial Considerations

Literature on submerged intakes is practically nonexistent between the mid 1950s and the end of the 1990s. Apparently, during this period, no works were developed related to the submerged inlets. The work performed in the 1940s and 1950s is, as could be expected, focused on experiments. The main goal of these works, which were conducted by the National Advisory Committee for Aeronautics (NACA), was to determine the influence of both the flow parameters and the geometric configuration on the performance parameters of this type of intake. The investigated flow parameters included the Mach number, the angle of attack, the mass flow rate or mass flow ratio, and the boundary-layer thickness. The influence of the main geometric configuration parameters (which include the inlet position, the lip angle, the shape of the ramp, and the boundary-layer deflectors) was assessed. Within the references reviewed, few had detailed information about the flowfield, which makes the comparison between the results described and a computational fluid dynamics (CFD) simulation impossible. Furthermore, despite the great amount of experimental work described in the references, the procedures were not always detailed. These studies identified the classical measures of performance of air intakes, which are the mass flow rate or mass flow ratio, the ram-recovery ratio, and the total drag coefficient. The mass flow ratio is the ratio of the actual mass flow ingested by the inlet to the mass flow that would enter to the intake at freestream conditions. The ram-recovery ratio is defined as the ratio between the dynamic pressure at the throat of the air inlet and the freestream dynamic pressure.

With the development of CFD techniques and the increasing computational power, recent studies involve both experimental and numerical efforts, mainly aiming to improve the inlet performance. In this respect, several performance improvement techniques were attempted. One of these attempts included the use of vortex generators to decrease the boundary-layer thickness that develops upstream of the air intake. There seems to be an opportunity for the performance improvement of secondary air inlets, which may be explored by the use of CFD techniques.

B. Early Works

Delany [4] tested a 1/4-scale model of a fighter-type airplane with two different locations of submerged inlets. NACA inlets with deflectors were also considered, as illustrated in Fig. 2.

High ram recovery was observed for all intakes located upstream of the wing, where the boundary layer is thinner. The ram recovery measured at the duct entrance was 0.960 for divergent walls with deflector extended forward, 0.970 for simple divergent walls, and 0.890 for parallel walls. This was a significant result, because for most configurations tested, the deflector increased the ram recovery about 0.005. The worst result obtained using divergent walls was better than the best result with parallel walls. The studies of flow characteristics indicated the formation of low-velocity regions near the ramp walls in the NACA inlets. Tuft tests showed that the airflow along the ramp followed the divergent walls, whereas the airflow along the fuselage was approximately parallel to the freestream flow. Consequently, at the top of the ramp walls there was a sudden change in the direction of airflow, which resulted in a rotational flow, as shown in Fig. 3. Also, it was found that the increase in drag with the deflectors may offset the advantage in ram recovery. It is believed that flow separation occurred in the aft portion of the deflector. To relieve the separation, the deflectors were extended forward, which led to a 40% reduction of the drag penalty.

Hall and Barclay [8] reported an experimental investigation of NACA submerged inlets at four locations on the fuselage of a fighter airplane model for Mach numbers from 0.30 to 0.875. The most important conclusions of the investigation were that 1) the ram-recovery ratio is greatly affected by variations in the mass flow ratio and 2) variations of Mach number and angle of attack, in general, cause small variations in the ram-recovery ratio.

Later, Hall and Frank [3] studied the influence of the inlet lip angle and the use of boundary-layer deflectors. The results indicated no change in the ram-recovery ratio for the range of lip angles tested. The authors of that study believed that the conditions under which the lip angle might have a large effect on the ram-recovery ratio were not obtained. The results also showed that the highest ram-recovery ratios are obtained with inlets in the forward location, and an increase of the boundary-layer thickness originates a decrease of the ram-recovery ratio. In addition, the use of the boundary-layer deflectors resulted in an increase of the maximum ram-recovery ratio and the mass flow ratio at which it occurred.

Mossman [9] tested two submerged inlets in a wind tunnel with parallel and divergent ramp walls. The range of Mach number was 0.2 to 0.94 for the parallel ramp inlet and 0.2 to 0.96 for the divergent ramp inlet. The divergent inlet works better at higher Mach numbers than the parallel inlet and has satisfactory pressure recovery. This was found to be due to the difference in the boundary-layer characteristics over the ramp. The highly three-dimensional flow through divergent inlets leads to a slower growth of the boundary layer, when compared with the quasi-two-dimensional flow found in parallel inlets. For both inlets, the decrease of ram recovery with decreasing mass flow ratio was attributed to the thickening of the boundary layer, which was a consequence of adverse pressure gradients along the ramp. For Mach numbers between 0.8 and 0.9, shock waves occurred on both of the inlets, which suggests that

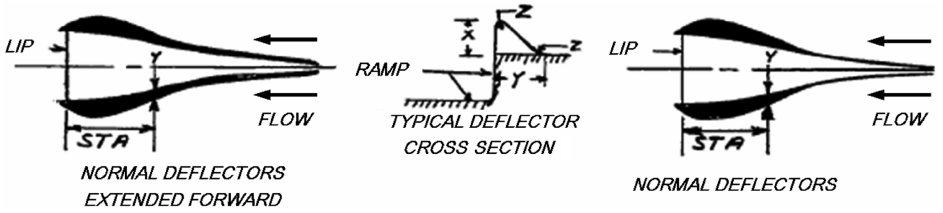

Fig. 2 Schematic representation of the flow defectors [4].

modifications of the inlet geometries could be attempted with the aim of displacing the shock wave toward the beginning of the ramp and thus reducing the amount of low-energy air ingested by the intake. In this circumstance, it could be expected that boundary-layer thickening would occur due to the shock/boundary-layer interaction [10].

Frank and Taylor [11] compared the transonic characteristics of a scoop-type inlet and a NACA submerged inlet. Wind-tunnel tests were conducted for both geometries at the same conditions. Tests were performed for Mach numbers from 0.79 to 1.12 and angles of attack of 0, 3, 6, and 9 deg. The results showed that although at low angle of attack and subsonic Mach numbers the submerged inlet had higher or equal ram-recovery ratio than the scoop inlet, increasing the angle of attack had a more adverse effect on the ram-recovery ratio of the submerged inlet than on that of the scoop inlet. The authors of that study attributed this result to the increasing strength of the vortex that formed off the lower ramp wall of the submerged inlet as the angle of attack was increased. Tests with a thicker boundary layer indicated that the losses in the ram-recovery ratio and mass flow ratios were greater for the scoop inlet. The mass flow ratio of the submerged inlet was practically unchanged under a thicker boundary layer.

Taylor [12] presents a comparative analysis of measurements of drag and ram-recovery ratio for a NACA submerged inlet and two other configurations resulting from modifications of its sidewalls. The investigation was conducted in a high-speed wind tunnel over a mass-flow-ratio range from 0 to 0.93 and Mach numbers between 0.8 and 1.11. Ram-recovery data indicated that the vortices formed above the diverging ramp walls, which entrained low-energy body boundary-layer air, resulting in reduced pressure recovery. The vortices are beneficial for their influence in thinning the boundary layer along the ramp floor, but upon entering the air-induction system, cause total pressure losses. To reduce the strength of the ramp-wall vortices and displace them outward, the inlet was modified by increasing the angle between the ramp floor and the walls to 134 and 146 deg, as shown in Fig. 4.

The results obtained indicated that the modified versions generally yield higher ram-recovery ratios than the NACA submerged inlet at the highest test mass flow ratio. This improvement in ram recovery was believed to be due to the outward displacement of the vortices generated by the ramp walls and the leakage of accumulated ramp-wall boundary layer that passed outside of the intake. Regarding the effects of Mach number and angle of attack, the comparisons indicated that for all angles of attack and Mach numbers tested, the two modified inlets generally yielded equal or superior ram-recovery ratios. Concerning the drag, no significant changes resulted from the modifications for Mach numbers below 1.0.

C. Recent Works

Devine et al. [2] investigated, both computationally and experimentally, the influence of a pair of vane-type vortex generators (geometry not presented) placed upstream of a parallel wall submerged inlet, such that the inlet lies downstream of the merging of the vortices. The measured values of the ram-recovery ratio were low when compared with previous published data; which the authors of that study believed to be due to the high ratio of boundary-layer thickness to inlet depth 1.42. The results also showed that the vortex downwash led to a thinning of the boundary layer and higher-energy air was forced into the inlet. Thus, the results, both

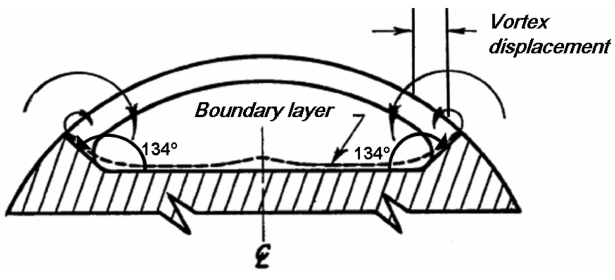

Fig. 4 Schematic representation of the 134-deg inlet [12].

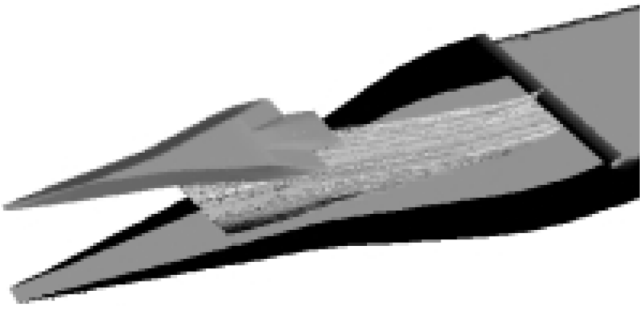

Fig. 5 NACA inlet with a delta wing vortex generator [1].

computational and experimental, showed an increase of 34 to 37% in terms of ram-recovery ratio.

A computational study of the influence of the use of a delta wing vortex generator, placed on the ramp of a NACA intake, such as shown in Fig. 5, on the performance of this type of inlets was performed by Faria and Oliveira [1]. The geometry considered was a flat plate of 10-m length with a NACA inlet in the center. The conventional inlet computed results were in good agreement with the expected values at the design point, in terms of ram-recovery ratio. Modifications in the basic vortex generator were also tested, regarding surface area, inclination, and axial position. In general terms, the results obtained were not satisfactory. The ram-recovery ratio decreased 5 to 23% when compared with the inlet without vortex generator, and the drag increased 25 to 53%.

Taskinoglu and Knight [13] investigated the flow of air vehicle submerged inlets through the use of numerical simulations. The computational work was conducted considering a generic inlet configuration at transonic flow conditions. The influence of the backpressure values was examined. The authors of that study observed that when backpressure is low enough for the flow to accelerate to supersonic speeds, a shock boundary-layer interaction occurs at the upper wall of the inlet. This creates flow distortion and total pressure loss downstream of the upper duct. However, if the backpressure is increased to maintain the flow upstream of the duct at subsonic speeds, the flow decelerates on the lower part of duct and swirls along the sidewalls. This, too, leads to a boundary-layer separation and flow distortion in the downstream part of the upper duct.

Taskinoglu and Knight [5] applied an automated shape optimization to a submerged subsonic inlet of an air vehicle to obtain higher quality of airflow at the compressor face. The chosen measures of airflow quality were the flow distortion and the swirl. The design variables of the optimization process were chosen to be the height, the length, and the angle of incidence of a fin, which was placed downstream of the inlet throat. The optimization study led to two optimal inlets and showed that the fin angle of incidence is the main parameter that determines the value of the swirl index. A fin protrusion with a positive incidence angle creates a high-pressure region over the upper surface of the fin. The pressure differential between lower and upper surfaces of the fin causes the formation of a tip vortex that accentuates the swirl, although creating a more axisymmetric flowfield, and hence lower circumferential distortion. A fin protrusion with a negative incidence angle, however, creates a lower-pressure region on the upper surface of the fin, resulting in a tip vortex formation in a direction opposite to the swirl direction of the baseline inlet, which reduces the swirl. The improvements obtained in this case with respect to the distortion level were not as good as in the previous case. Comparing the experimental results with those obtained numerically for the baseline inlet case, reasonable agreement was obtained in the low-velocity region associated with flow separation of boundary layer due to the duct curvature. Also, the maximum velocity values and velocity range are in very good agreement.

D. Current Design of the NACA Inlets

The design knowledge currently available for conventional NACA intakes comes from experimental results and is published by

Fig. 6 Schematic representation of a conventional NACA inlet cross section.

the Engineering Sciences Data Unit (ESDU) [14]. This database resulted from the compilation of a large number of empirical results that were obtained during the 1940s and 1950s. The main conclusions of the works developed during these years indicate that 1) an increase of the boundary-layer thickness originates a decrease of the ram-recovery ratio, 2) the ram recovery is greatly influenced by the variations of the mass flow rate, and 3) uniform and steady throat flows are required to obtain more efficient air inlets.

Currently, the design of a submerged NACA inlet with divergent ramp walls operating at maximum efficiency of dynamic pressure recovery is performed following the methodologies outlined in the ESDU. For a given flow condition, and based on preestablished parameters such as the inlet geometry (ramp shape, aspect ratio, and others), the boundary-layer thickness, the ram-recovery ratio, the mass flow rate, and the drag coefficient are determined from the ESDU.

Fig. 6 shows a schematic cross-sectional representation of a conventional NACA inlet in which the freestream conditions and the section of throat inlet are indicated.

One of the key parameters for the design of an air inlet is its ram-recovery ratio η_{fl}, which can be defined as [3,4]

$$\eta_{fl} = \frac{p_{t_{\mathrm{TH}}} - p_0}{p_{t_0} - p_0} \tag{1}$$

The variation of the ram-recovery ratio of an air inlet is usually expressed as a function of the mass flow ratio (MFR), which is defined as the ratio between the actual mass flow rate ingested by the inlet and the reference value $\dot{m}_0$, which corresponds to the maximum theoretical value that would be ingested by the intake at freestream conditions:

$$\dot{m}_0 = \rho_0 V_0 A_{\mathrm{TH}} \tag{2}$$

Another important parameter is the total drag coefficient C_{Dfl}, which results from the addition of two terms, the ram drag and the spillage drag. It is defined as follows:

$$C_{Dfl} = \frac{D}{(p_{t_0} - p_0) A_{\mathrm{TH}}} \tag{3}$$

Further details about these performance parameters of the conventional NACA inlets can be found in [14].

III. Numerical Approach

A. Flow Solver

All numerical simulations were conducted using the commercial CFD package FLUENT, Version 6.1 [15]. For the solution of the governing equations of the compressible flow, FLUENT uses a control-volume-based technique, which consists of the division of the domain into discrete control volumes using a computational grid. The integration of the governing equations on the individual control volumes allows constructing algebraic equations for the discrete dependent variables. The linearization of the discretized equations and solution of the resultant linear equation system yields updated values of the dependent variables.

In this work, an implicit segregated solver was used to solve the governing equations, along with a Spalart–Allmaras [16] turbulence model. The interpolation scheme used for the convection term was a second-order upwind scheme and a second order for calculating face pressure. The algorithm applied for pressure-velocity coupling was a semi-implicit method for pressure-linked equations (SIMPLE) [15].

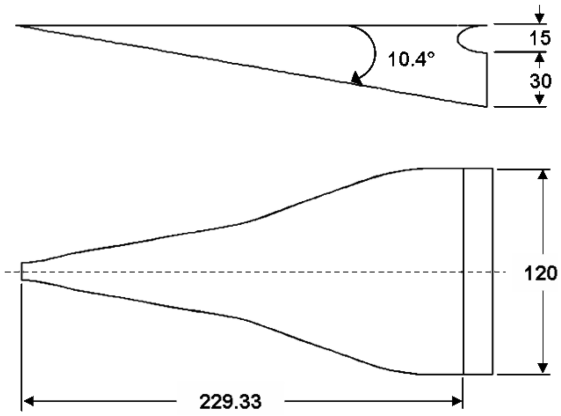

Fig. 7 NACA air inlet geometry (dimensions in mm).

B. Description of the Geometric Configurations

In this numerical study, four generic configurations are simulated and analyzed: the configuration with a conventional NACA intake, the configuration with a vortex generator type of delta wing, and the configuration resulting from the assembly of the conventional NACA inlet and the vortex generator with and without support.

1. *Conventional NACA Inlet*

The conventional NACA intake (geometric characteristics are shown in Fig. 7) is the first configuration studied in this work. This configuration corresponds to a typical air intake used in a regional transport aircraft. The flow conditions analyzed correspond to a Mach number of 0.31, an altitude of 9000 ft, and a temperature of −2.83°C. The results of this configuration will be used as a reference to evaluate the performance of the NACA intake when the vortex generator is used.

This conventional NACA intake is placed at the center of a flat plate of $10,000 \times 2000$ mm^2. The inlet is positioned at a distance of 5000 mm downstream of the beginning of the flat plate. To simulate actual flow conditions, an exit duct of rectangular cross section 120×30 mm^2 and 500-mm length is coupled to the NACA inlet throat. Because the assembly NACA inlet, flat plate, and exit duct are symmetrical with respect to the centerline of the NACA inlet, the configuration studied only considers half of the model. Thus, the computational domain consisted of a parallelepiped of $10,000 \times 1000 \times 1000$ mm^3, in which freestream conditions were established.

2. *Vortex Generator*

Two main considerations were accounted for in the design process of the vortex generator. First, the vortex generator geometry should be as simple as possible, and second, experimental results should be available to perform comparisons with the numerical results. Based on these considerations, a simple delta wing was chosen as the vortex generator, a classical configuration for which experimental results are available in the literature [17].

Schlichting and Truckenbrodt [17] present experimental lift coefficient curves, obtained for a Reynolds number of 7×10^5 for delta wings with a NACA0012 profile and different aspect ratios. These results show that the aspect ratio of 1.61 leads to the highest values of lift coefficient. Because lift is directly related to the vortex strength, this value of aspect ratio was chosen. Also, the same value of Reynolds number used in the experiments was used to determine the final dimensions of the vortex generator. Thus, considering the same flight conditions used in the design of the NACA inlet, the root chord of the vortex generator can be calculated as follows:

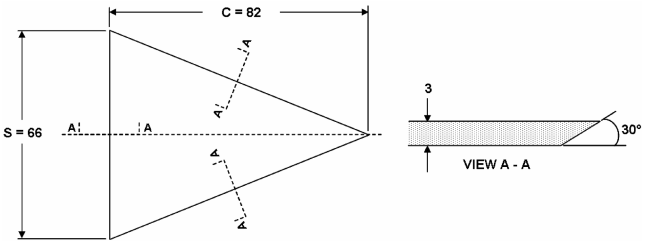

Fig. 8 Vortex generator geometry (dimensions in mm).

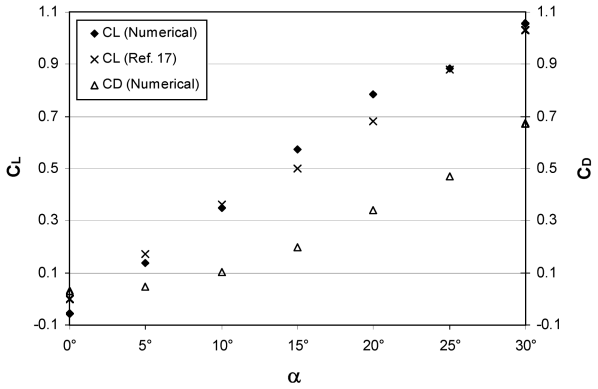

Fig. 9 C_L and C_D vs α; numerical and experimental results.

$$Re = \frac{V_0 C}{\upsilon} = 7 \times 10^5 = \frac{102C}{1.19 \times 10^{-5}} \rightarrow C = 82 \text{ mm} \qquad (4)$$

However, instead of using the thick NACA0012 profile, we decided for the sake of simplicity to design the vortex generator using a chamfered flat plate. The exact dimensions of the designed vortex generator are given in Fig. 8.

Computational results obtained for the isolated vortex generator at different values of angle of attack exhibited excellent agreement with the experimental lift coefficient curve, as shown in Fig. 9. This figure also shows the variations of the drag coefficient as a function of the angle of attack of the vortex generator.

3. NACA Inlet with Vortex Generator Without and with Support

The computational domain of the configuration NACA inlet with the freely standing vortex generator (i.e., vortex generator without its mast or support and corresponding to the NACA inlet with vortex generator and support) is identical to that used on the simulation of the conventional NACA intake. The only differences are the inclusion (in the first case) of the vortex generator and (in the second case) of the vortex generator and its support.

Three horizontal locations of the vortex generator were studied, placed upstream of the NACA inlet. For the configuration that led to the best results (ram-recovery ratio and mass flow rate), variations of the angle of attack and of the area of the vortex generator were performed. Finally, for this same configuration, the mast used to support the vortex generator was designed. Different sideslip angles

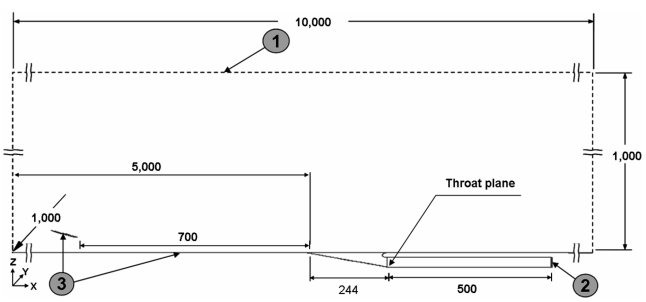

Fig. 10 Boundary condition setup for the NACA inlet with vortex generator; symmetry plane (dimensions in mm).

Table 1 Freestream conditions

Pressure p	Pa	72,428
Temperature T	K	270.3
Mach number M	——	0.31
Modified turbulent viscosity	m^2/s	0.001

of the support of the vortex generator were studied with the aim of evaluating its influence on the performance of the NACA inlet thus modified.

C. Boundary and Initial Conditions

The computational domain zones in which the boundary conditions were set are illustrated in Fig. 10. At the far field, zone 1, freestream conditions with a given Mach number, static pressure, and temperature were specified. At the duct exit section, zone 2, a constant static pressure was specified. No-slip adiabatic boundary conditions were set at the solid walls, zone 3. Finally, symmetry conditions were set at the symmetry plane of both the conventional NACA intake and the vortex generator.

The computations were initialized from the freestream conditions given in Table 1. In this table, the modified turbulent viscosity is the transported flow property in the Spalart–Allmaras [16] turbulence model. The value adopted for this property at the far-field boundary is also 0.001 m^2/s.

D. Mesh Generation

Grid generation of the studied configurations was performed using the commercial software ANSYS ICEM CFD, Version 5.0 [18]. All the meshes used in this work were structured meshes composed by hexahedral elements. The mesh of the conventional NACA intake with shell characteristics shown in Fig. 11 was composed of 255,000 elements.

An evaluation of the quality of the elements was performed using 1) the aspect ratio and 2) the angle of the elements as mesh quality parameters. For hexahedral elements, the aspect ratio is defined as the ratio of the distances between diagonally opposite vertices: longer diagonal and shorter diagonal. Thus, an aspect ratio of 1 corresponds to a perfectly regular element, and an aspect ratio of 0 indicates that the element has zero volume. The use of the quality parameter angle checks the maximum internal angle deviation from 90 deg for each cell. If the cells are distorted and the internal angles are small, the accuracy of the solution could be affected.

Figure 12, which shows the histogram of distribution of the number of elements as a function of the quality parameters' aspect ratio and angle, illustrates the quality of the mesh of the conventional NACA intake according to these two quality parameters. In this figure, it is possible to note that most of the elements of this mesh have an acceptable quality: aspect ratio near 1 and internal angle near 90 deg. However, it is clear that there are some elements (less than 1%) with a quality smaller than is desirable. These elements are

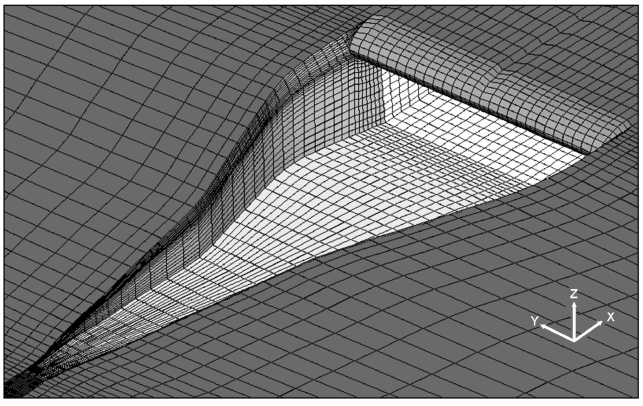

Fig. 11 Shell mesh of the conventional NACA inlet.

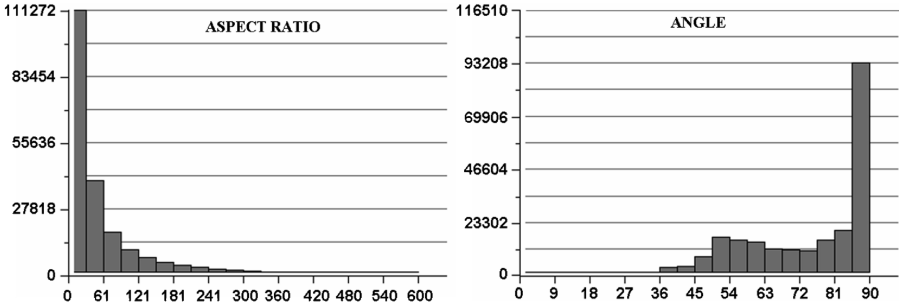

Fig. 12 Mesh quality of the conventional NACA inlet.

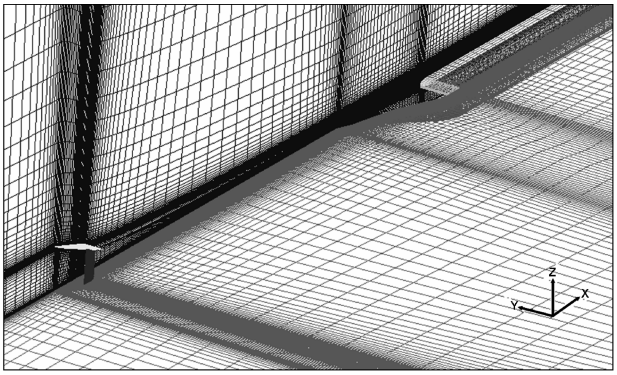

Fig. 13 Shell mesh of a generic configuration of NACA inlet and vortex generator and support.

mostly located in regions of the flow in which boundary layers are present. In the results section, it will be shown that the quality of this small group of elements does not affect the solution.

The computational mesh used to simulate the flow around the isolated vortex generator was composed of 600,000 elements, and the number of elements of the meshes corresponding to the configurations of NACA inlet with vortex generator consisted of 1,100,000 elements. The details of the meshes used to simulate the flow on these configurations of NACA inlet with vortex generator will not be shown, due to their similarity with those used at the configurations of NACA intake with vortex generator and support. The meshes used at these configurations of NACA intake with vortex generator and support, one of which is shown in Fig. 13, consisted of 1,700,000 elements. However, on all configurations corresponding to the NACA inlet with vortex generator, with and without support, an analysis was performed of mesh quality (similar to that performed on the conventional NACA inlet to verify the quality of the meshes used) to assure an appropriate description of the flow around the NACA inlet and the vortex generator.

IV. Results and Discussion

Table 2 summarizes the different configurations studied in this work. The area of the basic vortex generator is equal to 2706 mm^2.

Table 2 Summary of the configurations simulated

Case	HD, mm	α, deg	Area of the VG	β, deg
N1A-1		DATUM		——
NGVA	700	15	A	——
NGVB	500	15	A	——
NGVC	300	15	A	——
NGVA-25	700	25	A	——
NGVA-35	700	35	A	——
NGVA-1.5A	700	15	1.5A	——
NGVA-2.0A	700	15	2.0A	——
NGVAM-0	700	15	A	0
NGVAM-5	700	15	A	5
NGVAM-10	700	15	A	10

The vertical distance between the trailing edge of the vortex generator and the flat plate, in all configurations tested, was 50 mm. For the sake of simplicity, the results will be referenced to their respective codes, indicated in Table 2.

Regarding the convergence criterion of the simulated cases in this work, it is important to emphasize that in all of the computations performed here, the solver execution was interrupted only after the residuals of all the computed variables achieved their complete stabilization. The residual levels of all of the variables after the stabilization were of the order of 10^{-4} or less, except in the case of the mass conservation, in which the residuals were of the order of 10^{-2}. The approximate number of iterations necessary to achieve the complete stabilization of the residual was 6000, 10,000, and 25,000 for the configurations corresponding to the conventional NACA inlet, the NACA inlet with vortex generator, and the NACA inlet with vortex generator and support, respectively.

A. Conventional NACA Intake

1. Flow Structure

It is well known that the boundary-layer thickness is a determinant parameter of the efficiency of a NACA inlet. So, to characterize the influence of the vortex generator upon the boundary layer, plots representing the boundary-layer development upstream of the NACA inlet will be analyzed throughout the paper. Moreover, because the inlet efficiency is computed based on the throat flow, the distribution of the pressure coefficient along the throat plane of the NACA intake will be also shown. Figure 14 shows cross sections, in transverse planes to the external flow direction, of the longitudinal velocity contours for the configuration of the conventional NACA inlet, case N1A-1. This figure allows verifying the thick boundary that develops upstream of the NACA inlet. From these computations, it was determined that the boundary-layer thickness at the beginning of the ramp of the NACA intake is about 50 mm. Also, it is clear that the inlet ingests mostly low-energy fluid.

Figure 15 shows the distribution of the pressure coefficient along the throat plane of the NACA inlet. It is important to analyze the behavior of the pressure coefficient in this region, because the main performance parameter of the NACA inlet, the ram-recovery ratio, is

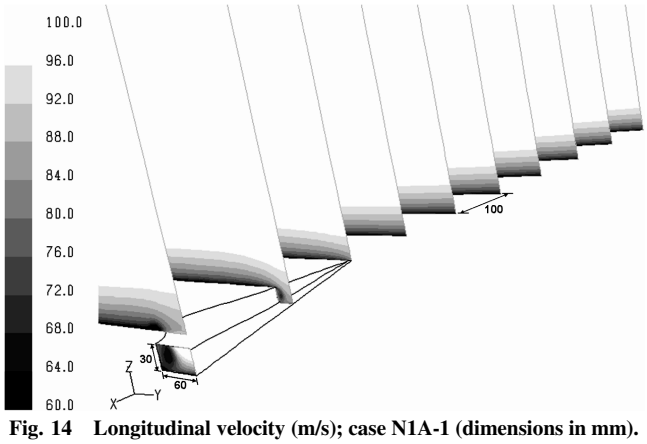

Fig. 14 Longitudinal velocity (m/s); case N1A-1 (dimensions in mm).

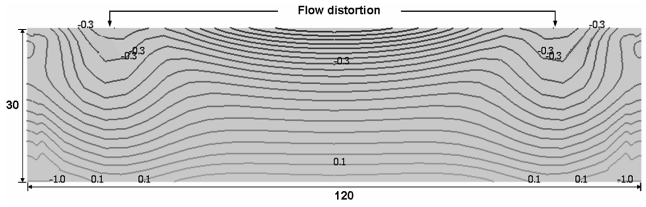

Fig. 15 Pressure coefficient; case N1A-1, throat plane of the NACA inlet (dimensions in mm).

defined as a function of the dynamic pressure on the throat plane of the NACA inlet. In this figure, the high level of flow distortion originated by the vortex formed above the divergent ramp walls can be clearly seen. Depending on the subsystem that is fed by this particular inlet, such a high level of flow distortion might be highly undesirable.

2. *Influence of the Level of Refinement of the Computational Mesh*

To analyze the influence of the level of refinement of the computational mesh used for the numerical simulations of the conventional NACA inlet on the values of its performance parameters, the mesh used was refined using one of the methods of solution-adaptive refinement available in FLUENT. The adaptive refinement process used is based on the use of a gradient adaption function, which is defined for a selected solution variable as being proportional to the ratio of the gradient at the element volume and the Euclidean norm of the gradient throughout the computational domain. Through the use of this gradient adaption function, it is assumed that maximum error occurs in high-gradient regions. This particular adaptive refinement process requires 1) the choice of the solution variable from which the adaption function will be constructed and 2) for this solution variable, the refinement threshold of the dimensionless adaption function from which the mesh will be refined by subdivision of its elements. Two adaptive refinement processes were performed in this work. The first refinement process was performed using the longitudinal component of the velocity as the solution variable. In this case, the refinement threshold was specified as equal to five (i.e., elements with adaption function values above this value were refined). In the second refinement process, the static pressure was considered as solution-variable. In the second case, the refinement threshold was specified as equal to 10. Modifications of these refinement thresholds, chosen after visual inspection of the refined mesh to assess their influence on the obtained results, were not performed.

The number of elements on the mesh after the adaptive refinement process based on the velocity gradient was 998,000, and 770,000 after the refinement process based on the static pressure gradient. It is worth recalling that the original mesh contained 255,000 elements. Figure 16 shows the meshes at the symmetry plane of the NACA inlet with and without adaptive refinement. In this figure, it is possible to verify that the refinement process increases the number of elements of the mesh at the regions in which the longitudinal component of the velocity and the static pressure present the greatest gradient (i.e., exit duct, ramp, and lip angle of the NACA inlet).

Table 3 shows the values of the performance parameters of the conventional NACA inlet that were computed from the results obtained from the numerical simulations for the configuration of the conventional NACA intake N1A-1 and for the cases in which the adaptive refinement processes were used. This table also shows the data used to design this particular NACA inlet. It is important to emphasize that the values of ram drag, shown in this table, were computed using the methodology prescribed by the ESDU 86002 [14]. The friction drag was calculated as the integral wall shear stress along the surfaces that define the NACA inlet only. Neither the flat plate nor the duct was considered for this drag calculation. The mass flow rate was obtained by a direct integration at the duct exit section of the NACA intake.

Table 3 shows that good agreement was obtained between the computed values of the performance parameters and the design data. Note that the value of the computed friction drag is negligible when it is compared with the value of the ram drag of the NACA inlet.

Even though the adaptive mesh refinement process more than doubles the number of elements, the resulting values of the performance parameters of the NACA inlet do not show significant discrepancies, as seen in Table 3. The results reported in this table show that the original mesh used to simulate the NACA inlet (i.e., the mesh without refinement) is already satisfactory to describe the flow behavior in the NACA inlet. When the mesh adaption process was performed, variations of only 1% (in terms of ram-recovery ratio [Eq. (1)], drag coefficient [Eq. (3)], and mass flow rate) were found. Therefore, the level of refinement used on the baseline mesh is considered satisfactory and will be applied to the different meshes used in the computations in which the vortex generator is included.

3. *Validation of the Numerical Results*

Because experimental results are not available to validate the numerical results obtained in this work, design data obtained from ESDU will be used as a reference to validate these computational results and to select the more appropriate turbulence model to

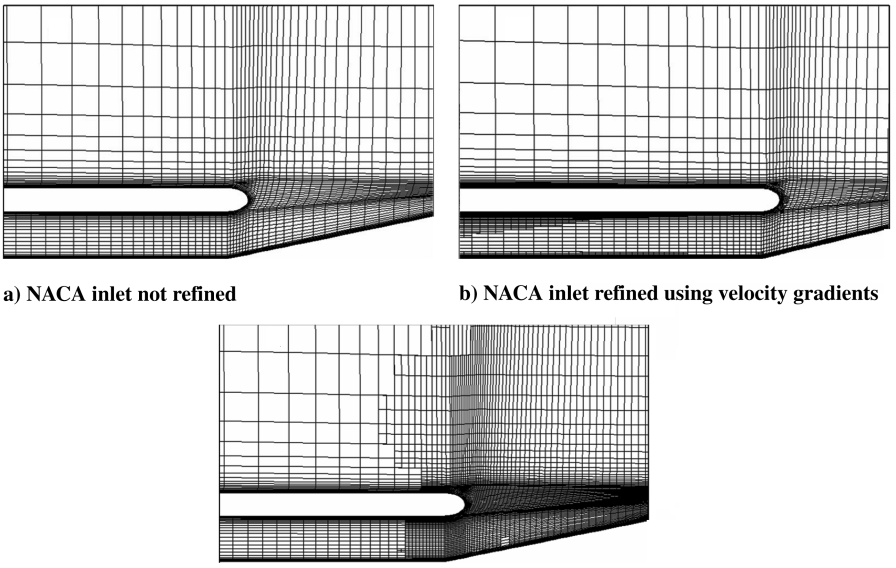

a) NACA inlet not refined

b) NACA inlet refined using velocity gradients

c) NACA inlet refined using pressure gradients

Fig. 16 Computational mesh without and with refinement; symmetry plane.

Table 3 Performance parameters: conventional NACA inlet with and without adaptive refinement

Parameters	Design data	N1A-1	Refinement: *X* velocity	Refinement: *S* pressure
Ram-recovery ratio	0.550	0.513	0.511	0.519
Mass flow rate, kg/s	0.260	0.260	0.259	0.261
Mass flow ratio	——	0.76	0.76	0.76
Total drag, *N*	16.41	18.60	18.45	18.59
Ram drag, *N*	——	18.13	17.97	18.11
NACA	——	18.13	17.97	18.11
VG	——	0.00	0.00	0.00
Support	——	0.00	0.00	0.00
Friction drag, *N*	——	0.47	0.48	0.47
NACA	——	0.47	0.48	0.47
VG	——	0.00	0.00	0.00
Support	——	0.00	0.00	0.00
Drag coefficient	0.93	1.06	1.06	1.06

simulate the flow in the NACA intake. Thus, Fig. 17 shows curves of ram-recovery ratio for the results obtained from the ESDU 86002 and from numerical simulations performed using the Spalart–Allmaras [16] and the k-ε eddy viscosity [19] turbulence models.

In Fig. 17, it is possible to verify that the numerical simulations always underestimate the values of the ram-recovery ratio of the NACA inlet. However, in this figure, one can observe that the performance trends computed with both turbulence models are quite similar, even if the semi-empirical figures computed from ESDU always exhibit higher values. Considering that the computed values of ram-recovery ratio using the Spalart–Allmaras turbulence model showed the smallest discrepancies (about 8%) when compared with the design data obtained from ESDU, and that it was specifically developed for aerodynamic applications, it was decided to use only this turbulence model in the simulations performed in this work.

B. NACA Inlet with the Freely Standing Vortex Generator

Before discussing the results corresponding to the NACA inlet with the freely standing vortex generator, it is important to indicate the rationale behind the initial positioning of the vortex generator. Because the vortex generator stall angle is about 35 deg, and to have an ample range of angles of attack, an angle of attack of 15 deg was chosen to perform the simulations. From results of simulations of the conventional NACA intake, it was determined that the boundary layer extended to a height of about 50 mm above the flat plate. Therefore, to capture and to mix freestream air with air within the boundary layer, it was decided that the trailing edge of the vortex generator should lie at a vertical distance of 50 mm from the flat plate. Regarding the horizontal position of the vortex generator with relation to the NACA inlet, it was determined with the aid of isosurfaces of vorticity that the lateral expansion of the vortex core is small (i.e., the regions with strong vorticity practically do not span beyond the vortex generator). The vortex core is therefore expected to delimit the region of the flowfield in which the influence of the vortex generator is strong.

Therefore, a crude model for the interaction between the vortex core and the NACA intake was presumed, in which the trajectory of the vortex is not influenced by the boundary layer, and thus an intersection between the vortex core and the plate can be easily computed. Note that the vortex decay due to viscous dissipation, which could also influence the choice of the position of the vortex generator with respect to the NACA intake, was also not accounted for. Using this model, three longitudinal positions were chosen for the vortex generator, as can be verified in Table 2. These positions correspond to distances between the trailing edge of the vortex generator and the beginning of the ramp of the inlet of 700, 500, and 300 mm. These positions would lead to an intersection between the vortex core and the flat plate upstream of, over, and downstream of the inlet, respectively.

1. *Flow Structure*

The influence of the use of the delta wing vortex generator upon the development of the boundary layer upstream of the NACA inlet can be assessed in Fig. 18, which shows cross sections, in transverse planes to the external flow direction, of the longitudinal velocity contours for the basic configuration of NACA inlet with vortex generator, called NGVA. In this figure, it is possible to see that the vortices generated by the delta wing vortex generator lead to a considerable reduction of the boundary-layer thickness upstream of the air intake. This substantial reduction takes place mainly at the central region of the flat plate. One immediate consequence of the reduction of the boundary-layer thickness is the larger amount of external air ingested by the NACA intake, which leads to increases of the ram-recovery ratio and the mass flow rate, as will be demonstrated later.

The pressure coefficient distribution along the throat plane of the NACA inlet for this configuration (NGVA) is shown in Fig. 19. Comparing this figure with Fig. 15, corresponding to case N1A-1, it

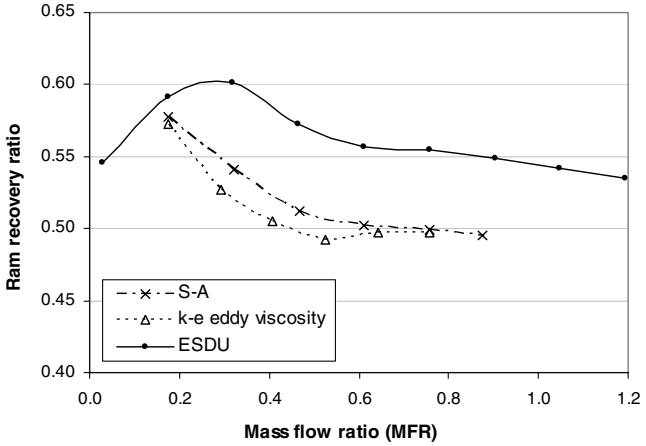

Fig. 17 Characteristic curve of ram-recovery ratio of the conventional NACA intake.

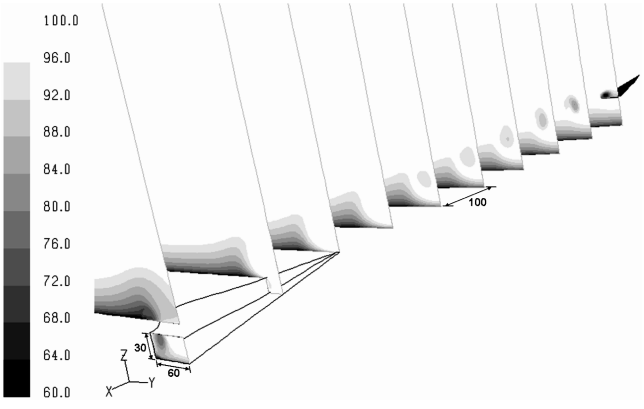

Fig. 18 Longitudinal velocity (m/s); case NGVA (dimensions in mm).

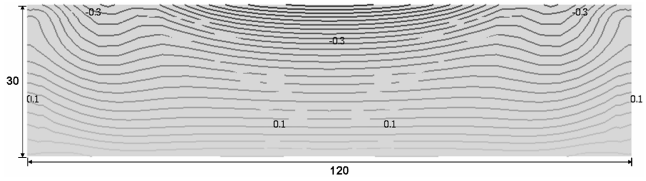

Fig. 19 Pressure coefficient; case NGVA, throat plane of the NACA inlet (dimensions in mm).

is possible to verify that the presence of the vortex generator produces a flow that is more uniform at the throat of the NACA intake. This decrease in flow distortion is also accompanied by an improvement of the performance parameters of the NACA intake, such as can be verified in Table 4.

2. Influence of the Horizontal Position of the Vortex Generator

The first parametric variation of the vortex generator geometry studied is the horizontal position of the vortex generator relative to the NACA intake. Two configurations, cases NGVB and NGVC, corresponding to the trailing edge of the vortex generator positioned at a horizontal distance from the ramp beginning of 500 and 300 mm, respectively, were analyzed. These configurations were obtained from variations of the basic configuration of NACA inlet with vortex generator, case NGVA.

Figures 20 and 21 show cross sections, in transverse planes to the external flow direction, of the longitudinal velocity contours for the configurations NGVB and NGVC, respectively. In these figures, it is possible to verify that the presence of the vortex generator still reduces the boundary-layer thickness, essentially at the central region of the flat plate. Comparing these figures with Fig. 18, case NGVA, it is observed that the reduction of the boundary-layer thickness is greater in the configuration corresponding to the farthest position of the vortex generator, case NGVA, and that even if the boundary-layer thickness increases as the vortex generator is placed closer to the NACA intake, it still remains much smaller than in the baseline case N1A-1 (Fig. 14).

The influence of the horizontal position of the vortex generator upon the distribution of the pressure coefficient on the throat plane of the NACA inlet is shown in Figs. 22 and 23 for cases NGVB and NGVC, respectively. These figures show that the reduction of the boundary-layer thickness observed in Figs. 20 and 21 is again accompanied by a decrease of the flow distortion on the throat plane of the NACA intake. Comparing these figures with Fig. 19, case NGVA, it is possible to note that the level of the flow distortion increases as the vortex generator is placed closer to the NACA intake.

Table 4 shows the values of the performance parameters for the conventional NACA intake (N1A-1), for the basic configuration of NACA inlet with vortex generator (NGVA), and for the two configurations of NACA inlet with vortex generator (NGVB and NGVC) that are being analyzed. The methodology of computation of these parameters is the same as described in the section on the conventional NACA inlet. The only difference is related to the

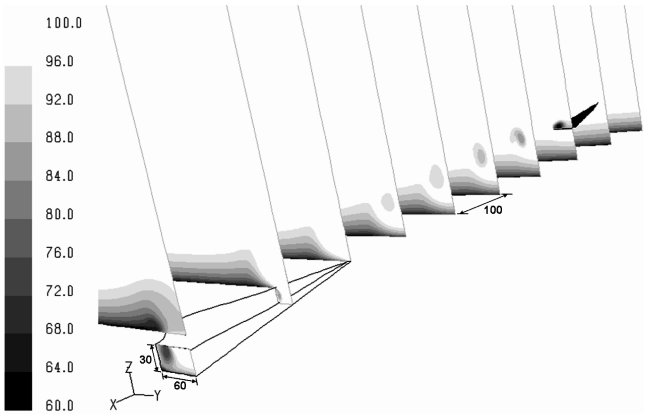

Fig. 20 Longitudinal velocity (m/s); case NGVB (dimensions in mm).

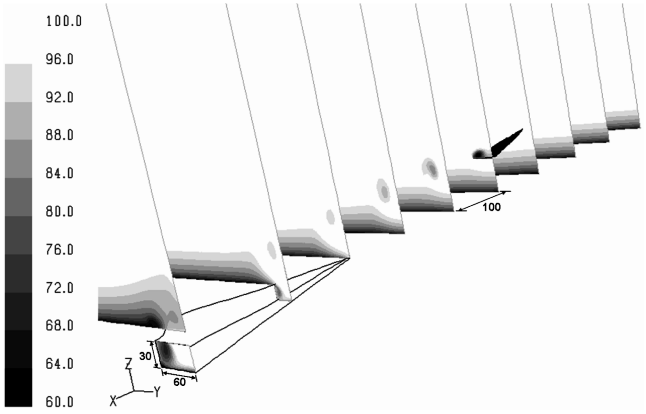

Fig. 21 Longitudinal velocity (m/s); case NGVC (dimensions in mm).

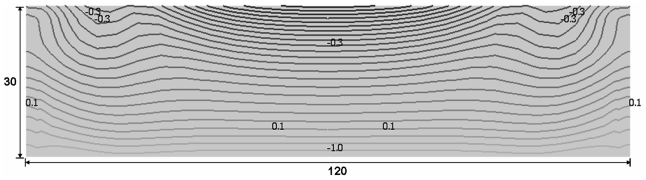

Fig. 22 Pressure coefficient; case NGVB, throat plane of the NACA inlet (dimensions in mm).

contribution of the vortex generator to both the ram drag and the friction drag. In this table, the percentage increases related to the values of the performance parameters corresponding to the conventional NACA inlet are indicated in parentheses.

The results shown in Table 4 indicate that the considerable reduction of the boundary-layer thickness upstream of the air intake,

Table 4 Performance parameters: influence of the horizontal position of the vortex generator

Parameters	Design data	N1A-1	NGVA	NGVB	NGVC
Ram-recovery ratio	0.550	0.513	0.741 (44.4%)	0.713 (39%)	0.647 (26.2%)
Mass flow rate, kg/s	0.260	0.260	0.302 (16%)	0.297 (14.2%)	0.294 (12.9%)
Mass flow ratio	——	0.76	0.88 (16%)	0.87 (14.2%)	0.86 (12.9%)
Total drag, *N*	16.41	18.60	32.43 (74.4%)	31.48 (69.3%)	29.08 (56.3%)
Ram drag, *N*	——	18.13	31.69 (74.7%)	30.77 (69.7%)	28.41 (56.7%)
NACA	——	18.13	29.68 (63.7%)	28.79 (58.8%)	26.43 (45.7%)
VG	——	0.00	2.01	1.98	1.98
Support	——	0.00	0.00	0.00	0.00
Friction drag, *N*	——	0.47	0.74 (60%)	0.71 (53.3%)	0.67 (43.4%)
NACA	——	0.47	0.59 (26.5%)	0.56 (19.8%)	0.51 (9.5%)
VG	——	0.00	0.16	0.16	0.16
Support	——	0.00	0.00	0.00	0.00
Drag coefficient	0.93	1.06	1.86 (74.4%)	1.8 (69.2%)	1.66 (56.3%)

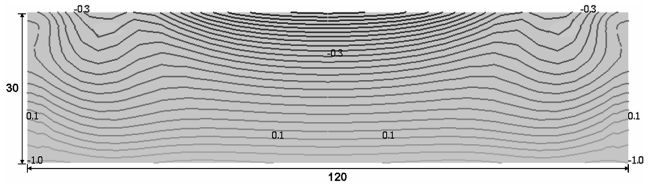

Fig. 23 Pressure coefficient; case NGVC, throat plane of the NACA inlet (dimensions in mm).

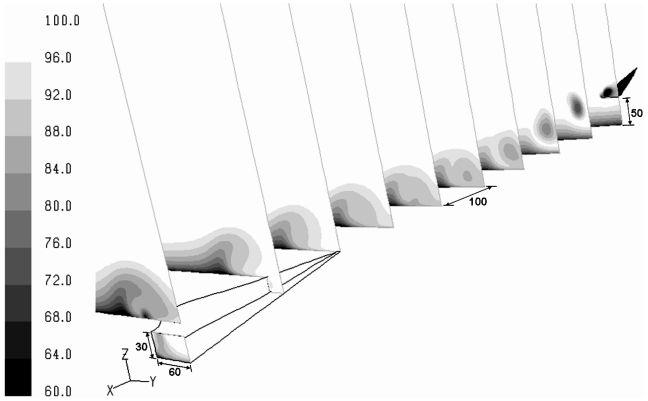

Fig. 24 Longitudinal velocity (m/s); case NGVA-25 (dimensions in mm).

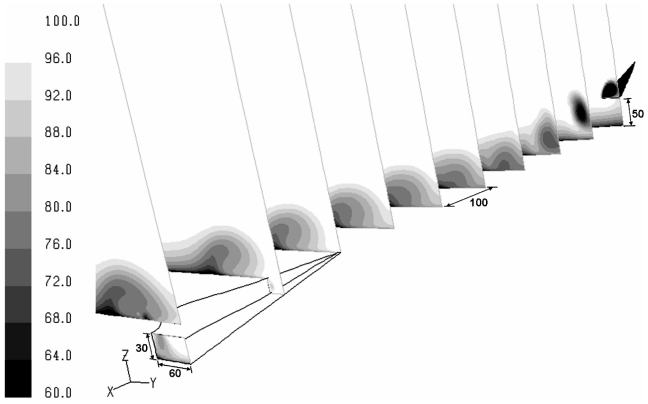

Fig. 25 Longitudinal velocity (m/s); case NGVA-35 (dimensions in mm).

observed in Fig. 18, leads to significant improvements of the ram-recovery ratio and the mass flow rate. This is a direct consequence of the larger amount of external air ingested by the NACA intake. Table 4 also shows that the three chosen horizontal positions of the vortex generator lead to significant improvements on the computed

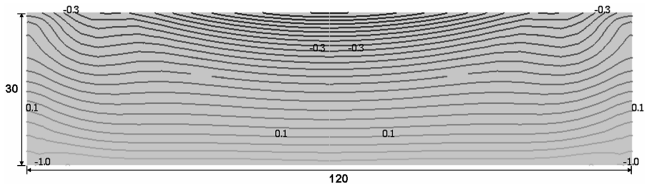

Fig. 26 Pressure coefficient; case NGVA-25, throat plane of the NACA inlet (dimensions in mm).

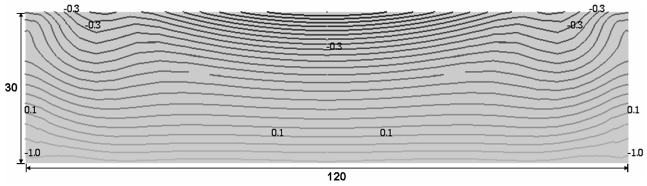

Fig. 27 Pressure coefficient; case NGVA-35, throat plane of the NACA inlet (dimensions in mm).

values of mass flow rate and ram-recovery ratio. The best results are obtained for the farthest-forward position of the vortex generator, case NGVA. As the vortex generator is displaced downstream, the gains decrease, but remain significant. Also in this table, a considerable increase of the drag coefficient is observed, which is related to both the increase of the mass flow rate and the decrease of the boundary-layer thickness. Thus, this drag coefficient increase is inevitable when the ram-recovery ratio increases. It is important to highlight that the drag contribution due to the vortex generator is about 7% of the total drag of the set.

3. Influence of the Angle of Attack of the Vortex Generator

A parametric variation of the angle of attack of the vortex generator is now presented. Two configurations, cases NGVA-25 and NGVA-35, corresponding to an angle of attack of the vortex generator of 25 and 35 deg, respectively, were analyzed. Note that these configurations were also obtained from variations of the basic configuration of NACA inlet with vortex generator, case NGVA.

Figures 24 and 25 show cross sections, in the same transverse planes to the external flow direction, of the longitudinal velocity contours for the configurations NGVA-25 and NGVA-35, respectively. A comparison of these figures with Fig. 18, case NGVA, shows that the boundary-layer development upstream of the NACA inlet and downstream of the vortex generator is certainly influenced by the increase of the angle of attack of the vortex generator. These figures also show that a stronger interaction between the counter-rotating vortices downstream of the vortex generator occurs as the angle of attack of the vortex generator is increased. This may be responsible for the observed decrease in performance that goes with the increase in the boundary-layer thickness and will be analyzed later on.

Table 5 Performance parameters: influence of the angle of attack of the vortex generator

Parameters	Design data	N1A-1	NGVA	NGVA-25	NGVA-35
Ram-recovery ratio	0.550	0.513	0.741 (44.4%)	0.754 (46.9%)	0.717 (39.7%)
Mass flow rate, kg/s	0.260	0.260	0.302 (16%)	0.304 (16.9%)	0.298 (14.6%)
Mass flow ratio	——	0.76	0.88 (16%)	0.89 (16.9%)	0.87 (14.6%)
Total drag, *N*	16.41	18.60	32.43 (74.4%)	36.65 (97%)	40.4 (117.2%)
Ram drag, *N*	——	18.13	31.69 (74.7%)	35.93 (98.1%)	39.71 (119%)
NACA	——	18.13	29.68 (63.7%)	30.01 (65.5%)	29.32 (61.7%)
VG	——	0.00	2.01	5.92	10.38
Support	——	0.00	0.00	0.00	0.00
Friction drag, *N*	——	0.47	0.74 (60%)	0.72 (54.2%)	0.69 (47.9%)
NACA	——	0.47	0.59 (26.5%)	0.57 (23.5%)	0.56 (19.8%)
VG	——	0.00	0.16	0.14	0.13
Support	——	0.00	0.00	0.00	0.00
Drag coefficient	0.93	1.06	1.86 (74.4%)	2.1 (97%)	2.31 (117.2%)

The influence of the angle of attack of the vortex generator on the pressure coefficient distribution along the throat plane of the NACA inlet is shown in Figs. 26 and 27, corresponding to the cases NGVA-25 and NGVA-35, respectively. When these figures are compared with Fig. 19, case NGVA, one can verify that the increase of the angle of attack of the vortex generator first originates a decrease and then an increase of the flow distortion along the throat plane of the NACA inlet. This deterioration of the flow uniformity at the throat, observed for high values of the angle of attack of the vortex generator, seems to be associated with the strong interaction between the counter-rotating vortex pair downstream of the vortex generator, which was observed in Figs. 24 and 25.

Table 5 shows the values of the performance parameters for the two configurations of NACA inlet with vortex generator, which were obtained from increases of the angle of attack of the vortex generator. The percentage increases related to the values of the performance parameters corresponding to the conventional NACA inlet are indicated in parentheses. The results shown in Table 5 indicate that the three angles of attack of the vortex generator simulated lead to significant improvements on the computed values of mass flow rate and ram-recovery ratio. Also, comparisons of these results show that a significant improvement is achieved in the values of mass flow rate and ram-recovery ratio when the vortex generator is set to a 25-deg angle of attack. However, when this angle is increased to 35 deg, there is a reduction in performance. This behavior indicates that it is possible to obtain, for a given configuration of NACA inlet and vortex generator, an optimum value for the angle of attack of the vortex generator.

It can be seen in Table 5 that the values of drag coefficient also exhibit a significant increase for the two configurations that are being analyzed. As already mentioned, this is a direct consequence of both the increase of mass flow rate and the decrease of the boundary-layer thickness. As expected, when the angle of attack of the vortex generator increases, so does the drag coefficient. However, the drag contribution due to the vortex generator is only about 25% of the total drag of the ensemble in the case of the highest angle of attack of the vortex generator.

4. *Influence of the Area of the Vortex Generator*

The last variation of the vortex generator configuration studied is the area of the vortex generator. Two configurations, cases NGVA-1.5A and NGVA-2.0A, corresponding to increases of 50 and 100% of the area of the vortex generator, respectively, were analyzed. In these configurations, which were obtained from variations of the basic configuration of NACA inlet with vortex generator, case NGVA, the aspect ratio of the vortex generator (i.e., $\Lambda = 1.61$) remained constant.

Figures 28 and 29 show cross sections, in transverse planes to the external flow direction, of the longitudinal velocity contours for the configurations NGVA-1.5A and NGVA-2.0A, respectively. Comparisons of these figures with Fig. 18, case NGVA, show that the increase of the area of the vortex generator increases the transverse extent of the region affected by the flow issued from the vortex generator. As a consequence, upstream of the NACA inlet, the width of the region of boundary-layer reduction increases around 50%, when comparing the configurations NGVA (Fig. 18) and NGVA-2.0A (Fig. 29). However, the central region between the NACA inlet and the vortex generator is not affected by the increase of the area of the vortex generator.

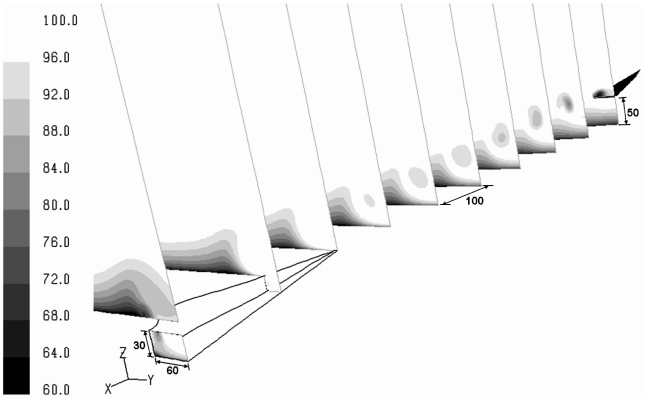

Fig. 28 Longitudinal velocity (m/s); case NGVA-1.5A (dimensions in mm).

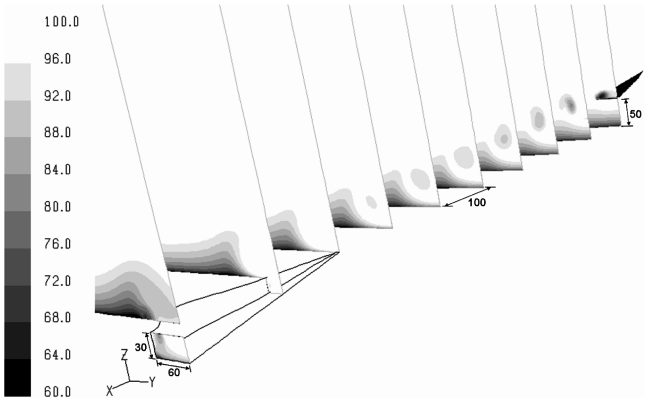

Fig. 29 Longitudinal velocity (m/s); case NGVA-2.0A (dimensions in mm).

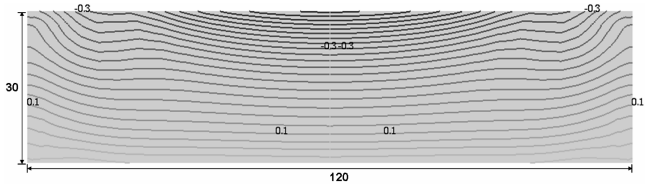

Fig. 30 Pressure coefficient; case NGVA-1.5A, throat plane of the NACA inlet (dimensions in mm).

The influence of the increase of the area of the vortex generator on the pressure coefficient distribution along the throat plane of the NACA inlet is shown in Figs. 30 and 31, which show results corresponding to the cases NGVA-1.5A and NGVA-2.0, respectively. A comparison of these figures with Fig. 19, case NGVA, shows that the increase of the area of the vortex generator produces a flow that is progressively more uniform at the throat plane of the NACA intake. This decrease in the level of flow distortion is believed to be related to the increase of the transverse extent of the region in which the boundary-layer thickness was reduced upstream of the NACA inlet, which was observed in Figs. 28 and 29.

The decrease on the level of flow distortion observed in Figs. 30 and 31 is accompanied by an increase of the performance parameters of the NACA intake, as shown in Table 6, which presents the values of the performance parameters for the two configurations of NACA inlet with vortex generator, which were obtained after increases in the area of the vortex generator. Also shown in this table are the percentage increases related to the values of the performance parameters corresponding to the conventional NACA inlet.

Comparing the results shown in Table 6 with those shown in Tables 4 and 5, it is possible to observe that the largest increases in the performance parameters of the NACA inlet are obtained for the vortex generators of increased area. Thus, a projected area 50%

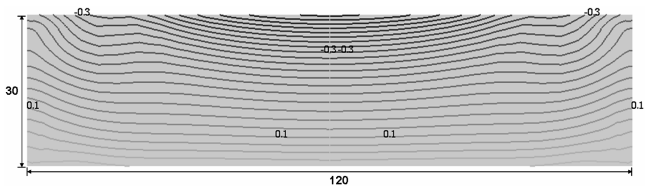

Fig. 31 Pressure coefficient; case NGVA-2.0A, throat plane of the NACA inlet (dimensions in mm).

Table 6 Performance parameters: influence of the area of the vortex generator

Parameters	Design data	N1A-1	NGVA	NGVA-1.5A	NGVA-2.0A
Ram-recovery ratio	0.550	0.513	0.741 (44.4%)	0.79 (54%)	0.808 (57.5%)
Mass flow rate, kg/s	0.260	0.260	0.302 (16%)	0.31 (19.3%)	0.313 (20.5%)
Mass flow ratio	——	0.76	0.88 (16%)	0.91 (19.3%)	0.91 (20.5%)
Total drag, *N*	16.41	18.60	32.43 (74.4%)	34.5 (85.5%)	36.02 (93.6%)
Ram drag, *N*	——	18.13	31.69 (74.7%)	33.69 (85.8%)	35.15 (93.8%)
NACA	——	18.13	29.68 (63.7%)	30.59 (68.7%)	30.9 (70.4%)
VG	——	0.00	2.01	3.10	4.25
Support	——	0.00	0.00	0.00	0.00
Friction drag, *N*	——	0.47	0.74 (60%)	0.81 (73.4%)	0.87 (86.5%)
NACA	——	0.47	0.59 (26.5%)	0.6 (28%)	0.6 (29.4%)
VG	——	0.00	0.16	0.21	0.27
Support	——	0.00	0.00	0.00	0.00
Drag coefficient	0.93	1.06	1.86 (74.4%)	1.97 (85.5%)	2.06 (93.6%)

larger leads to an increase of 54% for the ram-recovery ratio and 19.3% in the mass flow rate, and a projected area 100% larger enhances the performance of the NACA even further: 57.5% for the ram-recovery ratio and 20.5% for the mass flow ratio. This indicates that there exists a limit to the benefits obtained by an area increase. Considering that the penalty in terms of drag coefficient is lower in both cases than in the best case of the variation of the angle of attack, 25 deg, the process of increasing area seems to be the best route to improve the performance of the NACA intakes. Another favorable aspect of this type of parametric variation is the small contribution of the vortex generator to the total drag of the ensemble, only about 10%, in the case for which the area of the vortex generator is increased by 100%.

C. NACA Inlet with Vortex Generator and Support

The next stage in the development of our work was to design the support of the vortex generator that is used to maintain the desired relative position with respect to the NACA intake. To this end, it was considered that the support should, if possible, contribute to the reduction of boundary-layer thickness upstream of the NACA intake and downstream of the vortex generator. Considering this aspect, the support needs to be designed so that the wake generated by the support can contribute positively to the effect of the counter-rotating vortices generated on the suction side of the vortex generator and, specifically, to supplement the effect of these vortices on the reduction of the boundary-layer thickness. Because the reduction of the boundary-layer thickness occurs mainly at the central region of the flat plate, it was decided to use a pair of tip-mounted supports. Another possibility considered was the use of a ventral support, which was rejected because the wake generated by this type of support could 1) negatively influence the process of reducing the boundary-layer thickness and 2) be ingested by the NACA intake, degrading its performance parameters.

The basic configuration of NACA intake with vortex generator, called NGVA, was used as the configuration on which the support was designed. The designed support, which is shown in Fig. 32, was obtained as a result of the extrusion, at the normal direction to the flat plate, of a NACA0012 profile with a 25-mm chord. The lateral distance between the leading edge of the support and the symmetry plane of the vortex generator is 21 mm. Defining the angle formed by the chord of the support and the symmetry plane of the vortex generator as the sideslip angle, it was decided to perform computations for different values of the sideslip angle, to evaluate its influence on the performance parameters of the NACA inlet. Note that it is expected that the actual flow sideslip angle should be different from the geometrical sideslip, because the pressure difference between the suction and the pressure side of the vortex generator induces lateral flow.

1. *Flow Structure*

Figure 33 shows cross sections of the longitudinal velocity contours for the basic configuration of NACA inlet with vortex generator and support, NGVAM-0. Comparing this figure with Fig. 18, corresponding to the basic configuration of NACA inlet with vortex generator, it is possible to see that the boundary-layer development upstream of the NACA inlet and downstream of the vortex generator is slightly influenced by the presence of the support of the vortex generator. This influence seems to be restricted to the first 200 mm downstream of the vortex generator, where a reduction of the velocity due to the wake generated by the support occurs. Further downstream of the vortex generator, the boundary-layer thickness does not present significant variations due to the presence of the support. Thus, the use of the vortex generator and its support continues to lead to a considerable reduction of the boundary-layer

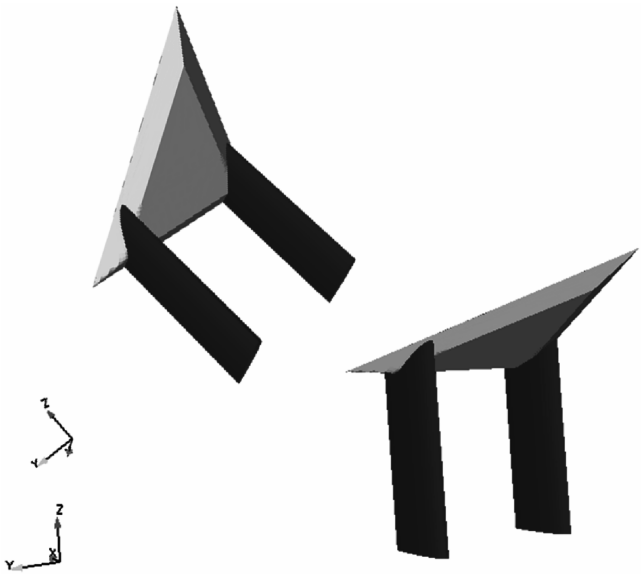

Fig. 32 Schematic view of the vortex generator and support.

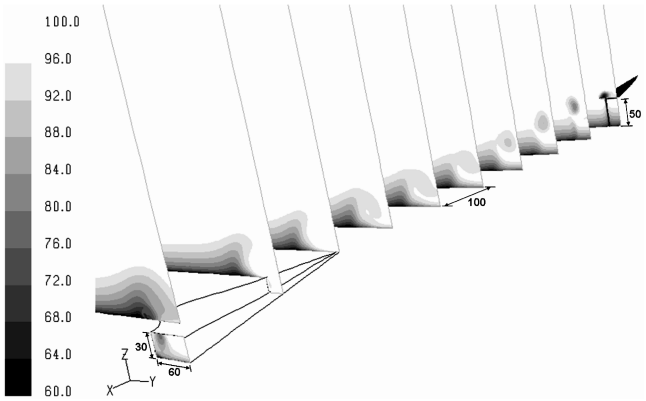

Fig. 33 Longitudinal velocity (m/s); case NGVAM-0 (dimensions in mm).

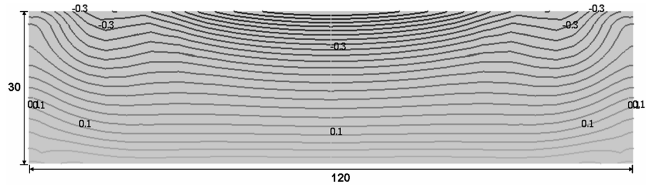

Fig. 34 Pressure coefficient; case NGVAM-0, throat plane of the NACA inlet (dimensions in mm).

thickness upstream of the air intake, and significant improvements in the performance parameters of the NACA intakes are obtained.

The pressure coefficient distribution along the throat plane of the NACA inlet for this basic configuration of NACA inlet with vortex generator and support is shown in Fig. 34. Comparing this figure with Fig. 19, corresponding to the case NGVA, it is possible to verify that the presence of the support of the vortex generator produces a flow that is slightly more uniform at the throat of NACA inlet. This decrease in flow distortion is accompanied by an increase of the performance parameters of NACA intake, such as is shown in Table 7.

2. *Influence of the Sideslip Angle of the Support of the Vortex Generator*

To assess the influence of the sideslip angle of the vortex generator support on the performance parameters of the NACA intake, two different values of the support sideslip angle (5 and 10 deg, configurations NGVAM-5 and NGVAM-10) were studied.

Figures 35 and 36 show cross sections of the longitudinal velocity contours for the configurations NGVAM-5 and NGVAM-10, respectively. In these figures, it is possible to verify that for the two values of the sideslip angle of the support (i.e., $\beta = 5$ and 10 deg), the reduction of the boundary-layer thickness at the central region of the flat plate practically remains unaltered. These figures also show that the wake of the support seems to enhance the vertical motion of the fluid downstream of the vortex generator.

The influence of the vortex generator support sideslip angle on the distribution of the pressure coefficient on the throat plane of the NACA inlet is shown in Figs. 37 and 38 for the cases NGVAM-5 and NGVAM-10, respectively. In these figures, it is possible to see that the increases of the vortex generator support sideslip angle produce a flow that is progressively more uniform at the throat of the NACA inlet. This decrease in flow distortion is accompanied by an increase of the performance parameters of NACA intake, as observed in Table 7.

Indeed, Table 7 shows the values of the performance parameters for the conventional NACA intake (N1A-1), for the basic configuration of the NACA inlet with vortex generator without and with support (NGVA and NGVAM-0), and for the two configurations of the NACA inlet with vortex generator and support (NGVAM-5 and NGVAM-10) that are being analyzed. These parameters were computed following the same procedures used for the conventional NACA inlet, but now accounting for the contribution of the vortex generator and its support to both the ram

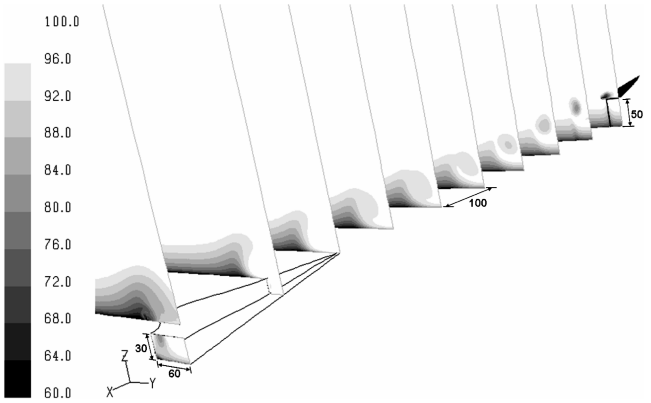

Fig. 35 Longitudinal velocity (m/s); case NGVAM-5 (dimensions in mm).

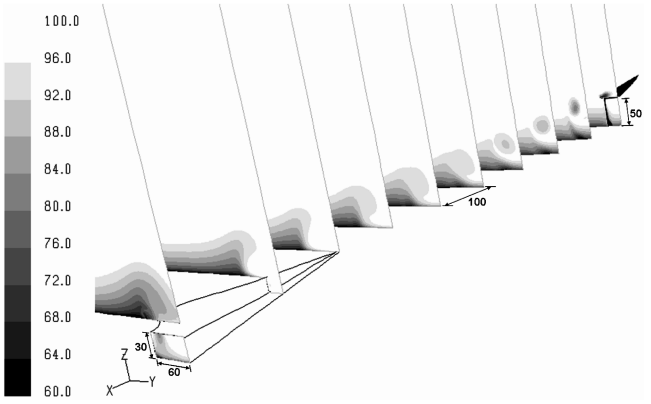

Fig. 36 Longitudinal velocity (m/s); case NGVAM-10 (dimensions in mm).

drag and the friction drag. In this table, the percentage increases related to the values of the performance parameters corresponding to the conventional NACA inlet are indicated in parentheses.

The results shown in Table 7 indicate that the presence of the support does not negatively affect the values of the performance parameters of the NACA intake. On the contrary, it contributes to an increase in the overall performance of the intake. Thus, this table shows that the three configurations of the NACA inlet with vortex generator and support exhibit improvements for the computed values of mass flow rate and ram-recovery ratio. The largest increases in these performance parameters are obtained for a sideslip angle of the support equal to 10 deg.

In Table 7, it can be seen that in the three configurations of NACA inlet with vortex generator and support, the drag coefficient values exhibit a small increase when compared with the corresponding values of the case called NGVA. The reason behind this slight

Table 7 Performance parameters: influence of the sideslip angle of support of the vortex generator

Parameters	Design data	N1A-1	NGVA	NGVAM-0	NGVAM-5	NGVAM-10
Ram-recovery ratio	0.550	0.513	0.741 (44.4%)	0.749 (46%)	0.774 (50.9%)	0.787 (53.3%)
Mass flow rate, kg/s	0.260	0.260	0.302 (16%)	0.303 (16.5%)	0.307 (18.1%)	0.309 (18.9%)
Mass flow ratio	——	0.76	0.88 (16%)	0.88 (16.5%)	0.9 (18.1%)	0.9 (18.9%)
Total drag, *N*	16.41	18.60	32.43 (74.4%)	33.18 (78.4%)	33.67 (81%)	34.31 (84.5%)
Ram drag, *N*	——	18.13	31.69 (74.7%)	32.34 (78.3%)	32.8 (80.9%)	33.45 (84.4%)
NACA	——	18.13	29.68 (63.7%)	29.81 (64.4%)	30.22 (66.7%)	30.43 (67.8%)
VG	——	0.00	2.01	2.35	2.21	2.09
Support	——	0.00	0.00	0.18	0.37	0.93
Friction drag, *N*	——	0.47	0.74 (60%)	0.84 (80.1%)	0.86 (85.8%)	0.87 (86%)
NACA	——	0.47	0.59 (26.5%)	0.58 (24.2%)	0.59 (26.8%)	0.6 (29.2%)
VG	——	0.00	0.16	0.15	0.15	0.15
Support	——	0.00	0.00	0.11	0.13	0.11
Drag coefficient	0.93	1.06	1.86 (74.4%)	1.9 (78.4%)	1.93 (81%)	1.96 (84.5%)

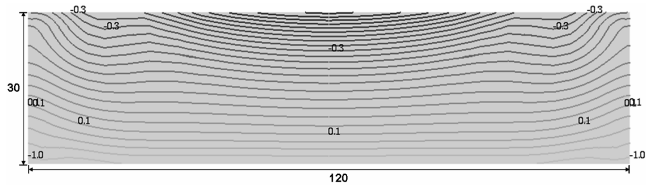

Fig. 37 Pressure coefficient; case NGVAM-5, throat plane of the NACA inlet (dimensions in mm).

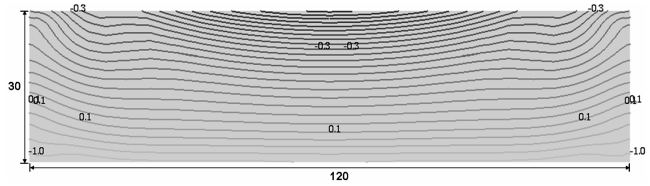

Fig. 38 Pressure coefficient; case NGVAM-10, throat plane of the NACA inlet (dimensions in mm).

increase observed is related to the fact that the contribution to the ram drag, the main component of the total drag, due to the presence of the support is negligible when compared with that of the NACA inlet. However, when the values of the drag coefficient of the configurations of NACA inlet with vortex generator and support are compared with that of the conventional NACA inlet, it is possible to see that the obtained increases are considerable. This is a direct consequence of the increase of mass flow rate that follows the reduction of the boundary-layer thickness. The drag contribution due to the vortex generator with support is only about 10% of the total drag of the ensemble. In this case, 7% corresponds to the drag produced by the vortex generator and 3% by the support of the vortex generator.

V. Conclusions

The literature review performed to establish the state of the art of the so-called submerged air inlets indicated that the boundary-layer thickness upstream of the air intake is the key parameter governing the performance of this type of inlet, and that the larger the boundary-layer thickness, the poorer the performance of the air inlet. Thus, in this computational work, the influence of a delta wing vortex generator on the boundary layer that develops upstream of a submerged air intake was investigated with the aim of decreasing its thickness to improve the performance of the air inlet.

The values of the ram-recovery ratio of the conventional NACA inlet computed from the results obtained from numerical simulations show that there is a good agreement when compared with their respective design data. The results also show that the adopted refinement process does not have a significant influence on the results obtained. The approximately 1% differences obtained relative to the original mesh show that the spatial discretization errors are small.

Computational results show that in all configurations, the presence of the freely standing vortex generator produces considerable reductions of the boundary-layer thickness and significant improvements of the performance parameters of the NACA inlet. The improvements in ram-recovery ratio and mass flow rate relative to the conventional NACA intake are as much as 58 and 21%, respectively. When the vortex generator support was used, additional improvements in the performance parameters of the NACA inlet were obtained. In this case, ram-recovery-ratio improvements up to 53% and intake mass-flow-rate improvements up to 19% were achieved. The contribution of the drag induced by the presence of the vortex generator with support on the total drag of the ensemble is small, only about 10%.

To validate the results obtained in this work, an associated experimental study is needed in which detailed measurements would allow validation of these numerical results. Future work should also involve the study of other parametric variations, including combinations of those already studied, as well as the overall sideslip angle of the intake, to optimize the vortex generator geometry.

Acknowledgments

The authors wish to thank Empresa Brasileira de Aeronáutica, Conselho Nacional de Desenvolvimento Cientifico e Tecnológico, and Fundação de Amparo à Pesquisa do Estado de São Paulo for the support provided for this work. During this work Luís Fernando Figueira da Silva was on leave from the Laboratoire de Combustion et de Détonique (Centre National de la Recherche Scientifique, France). Leticia Hime participated in the state-of-the-art studies and the vortex generator definition. Mesh generation was performed by Rodrigo Ferraz of ESSS (Engineering Simulation and Scientific Software Ltda.).

References

[1] Nogueira de Faria, W., and Oliveira, G. L., "Análise de Entradas de Ar tipo NACA com Gerador de Vórtices," 9th Brazilian Congress of Thermal Engineering and Sciences (ENCIT 2002), Brazilian Society of Mechanical Engineering and Sciences, Paper CIT02-0758, 2002.

[2] Devine, R. J., Watterson, J. K., Cooper, R. K., and Richardson, J., "An Investigation into Improving the Performance of Low Speed Auxiliary Air Inlets Using Vortex Generators," 20th AIAA Applied Aerodynamics Conference, St. Louis, MO, AIAA Paper 2002-3264, June 2002.

[3] Hall, C. F., and Frank. J. L., "Ram-Recovery Characteristics of NACA Submerged Inlets at High Subsonic Speeds," NACA RM A8I29, Nov. 1948.

[4] Delany, N. K., "An Investigation of Submerged Air Inlets on a 1/4-Scale Model of a Fighter-Type Airplane," NACA RM A8A20, June 1948.

[5] Taskinoglu, E. S., and Knight, D., "Multi-Objective Shape Optimization Study for a Subsonic Submerged Inlet," *Journal of Propulsion and Power*, Vol. 20, No. 4, 2004, pp. 620–633.

[6] Gorton, S. A., Owens, L. R., Jenkins, L. N., Allan, B. G., and Schuster, E. P., "Active Flow Control on a Boundary-Layer Ingesting Inlet," 42nd AIAA Aerospace Sciences Meeting and Exhibit, Reno, NV, AIAA Paper 2004-1203, Jan. 2004.

[7] Mossman, E. A., and Randall, L. M., "An Experimental Investigation of the Design Variables for NACA Submerged Duct Entrances," NACA RM A7130, Jan. 1948.

[8] Hall, C. F., and Barclay, F. D., "An Experimental Investigation of NACA Submerged Inlets at High Subsonic Speeds. I-Inlets Forward of the Wing Leading Edge," NACA RM A8B16, June 1948.

[9] Mossman, E. A., "A Comparison of Two Submerged Inlets at Subsonic and Transonic Speeds," NACA RM A9F16, Sept. 1949.

[10] Shapiro, A. H., *The Dynamics and Thermodynamics of Compressible Fluids Flow*, Wiley, New York, 1976.

[11] Frank, J. L., and Taylor, R. A., "Comparison of Drag, Pressure Recovery, and Surface Pressure of a Scoop-Type and an NACA Submerged Inlet at Transonic Speeds," NACA RM A51H20a, Dec. 1951.

[12] Taylor, R. A., "Some Effects of Side-Wall Modifications on the Drag and Pressure Recovery of an NACA Submerged Inlet at Transonic Speeds," NACA RM A51LO3a, Feb. 1952.

[13] Taskinoglu, E. S., and Knight, D., "Numerical Analysis of Submerged Inlets," 20th AIAA Applied Aerodynamics Conference, St. Louis, MO, AIAA Paper 2002-3147, June 2002.

[14] "Drag and Pressure Recovery Characteristics of Auxiliary Air Inlets at Subsonic Speeds," Engineering Sciences Data Unit, Rept. 86002 with Amendments A and B, London, 1996.

[15] FLUENT, Flow Modeling Software, Ver. 6.1, Fluent, Inc., Lebanon, NH, 2003.

[16] Spalart, P. R., and Allmaras, S. R., "A One-Equation Turbulence Model for Aerodynamic Flows," *La Recherche Aérospatiale*, No. 1, 1994, pp. 5–21.

[17] Schlichting, H., and Truckenbrodt, E., *Aerodynamics of the Airplane*, McGraw–Hill, New York, 1979.

[18] ANSYS ICEM CFD, Software Package, Ver. 5.0, ANSYS, Inc., Berkeley, CA, 2003.

[19] Shih, T. H., Liou, W. W., Shabbir, A., and Zhu, J., "A New k-Eddy-Viscosity Model for High Reynolds Number Turbulent Flows—Model Development and Validation," *Computers and Fluids*, Vol. 24, No. 3, 1995, pp. 227–238.